

# Static Quark Potential and the Renormalized Anisotropy on Tadpole Improved Anisotropic Lattices<sup>1</sup>

Wei Liu<sup>a</sup>, Ying Chen<sup>b</sup>, Ming Gong<sup>a</sup>, Xin Li<sup>a</sup>, Chuan Liu<sup>a</sup>,  
and Guozhan Meng<sup>a</sup>

<sup>a</sup>*School of Physics, Peking University  
Beijing, 100871, P. R. China*

<sup>b</sup>*Institute of High Energy Physics  
Academia Sinica, P. O. Box 918  
Beijing, 100039, P. R. China*

---

## Abstract

Static quark potential is studied using a tadpole improved gauge lattice action. The scale is set using the potential for a wide range of bare parameters. The renormalized anisotropy of the lattice is also measured.

*Key words:* Non-perturbative renormalization, improved actions, anisotropic lattice.

*PACS:* 12.38.Gc, 11.15.Ha

---

## 1 Introduction

It has become clear that anisotropic lattices and improved lattice actions greatly facilitate lattice QCD calculations involving heavy physical objects like the glueballs, one meson states with non-zero three momenta and multi-meson states with or without three momenta. It is also a good workplace for the study of hadrons with heavy quarks. In many of the lattice calculations, it

---

<sup>1</sup> This work is supported by the Key Project of National Natural Science Foundation of China (NSFC) under grant No. 10235040, No. 10421503, and supported by the Trans-century fund and the Key Grant Project of Chinese Ministry of Education (No. 305001).

is useful to use finite size techniques in which lattices with fixed physical volumes are simulated. For the purpose of these calculations, one needs to know the correspondence between the lattice spacing in physical units and the bare gauge coupling  $\beta$ . It is also important to check the renormalization effects of the anisotropy parameter for these actions. In this work we present our numerical studies on these issues using the tadpole improved gluonic action on asymmetric lattices:

$$\begin{aligned}
S = & -\beta \sum_{i>j} \left[ \frac{5}{9} \frac{\text{Tr}P_{ij}}{\xi_0 u_s^4} - \frac{1}{36} \frac{\text{Tr}R_{ij}}{\xi_0 u_s^6} - \frac{1}{36} \frac{\text{Tr}R_{ji}}{\xi_0 u_s^6} \right] \\
& -\beta \sum_i \left[ \frac{4}{9} \frac{\xi_0 \text{Tr}P_{0i}}{u_s^2} - \frac{1}{36} \frac{\xi_0 \text{Tr}R_{i0}}{u_s^4} \right]
\end{aligned} \tag{1}$$

where  $P_{ij}$  is the usual plaquette variable and  $R_{ij}$  is the  $2 \times 1$  Wilson loop on the lattice. The parameter  $u_s$ , which we take to be the fourth root of the average spatial plaquette value, incorporates the usual tadpole improvement [1] and  $\xi_0$  designates the bare aspect ratio of the anisotropic lattice. With the tadpole improvement in place, the bare anisotropy parameter  $\xi_0$  suffers only small renormalization. Therefore, the physical, or renormalized anisotropy parameter  $\xi$ , which can be determined by comparing physical quantities which depend on distances in both the spatial and the temporal directions, will be quite close to its bare value  $\xi_0$ . The effect of this renormalization will be studied in this paper for various values of  $\beta$  using the so-called side-way potential method. Using the pure gauge action (1), glueball and light hadron spectrum has been studied within the quenched approximation [2,3,4,5,6,7,8].

In this paper, we will study the static quark anti-quark potential using the pure gauge action given in Eq. (1). The static quark anti-quark potential is obtained by the measurement of the Wilson loops on the lattice. Then, we set the scale in physical unit using the Sommer scale  $r_0$  which is defined via the static quark potential. This establishes the relation between the lattice spacing and the bare gauge coupling. For all the  $\beta$  values we studied, we also investigate the renormalized anisotropy parameter  $\xi$  using the side-way potential method. Similar studies have been carried out before [9,10]. Our study covers more parameter space which is used in anisotropic lattice simulations. The renormalized anisotropy is also calculated within perturbation theory to one-loop [11].

This paper is organized in the following manner. In Section 2, parameters of our simulations are given and the details of the Wilson loop measurements are presented. From these data, we extract the static quark potential and the lattice spacing is determined in terms of the physical scale  $r_0$ . The results for all  $\beta$  are then interpolated using quadratic polynomials. These interpolation then offers a rather precise correspondence between  $\beta$  and  $r_0/a_s$  over the whole

range of  $\beta$  that have been simulated. In section 3, we discuss the side-way potential measurements which yield the renormalized anisotropy for all our simulation points. In Section 4, we will conclude with some general remarks.

## 2 Simulation Results for Static Potential

In this section, we present our numerical results for the study of the static quark anti-quark potential for various gauge coupling  $\beta$ . Our values of  $\beta$  range from 1.9 to 2.8 which roughly corresponds the lattice spacing  $a_s$  in the range of 0.35fm to 0.12fm. Details of the simulation parameters are summarized in Table 1.

Since we are interested in the spatial lattice spacing in physical unit, which is sensitive to the ultra-violet physics, we therefore only use small lattices of size  $8^3 \times 40$ . The lattices are generated using the conventional Cabbibo-Mariani pseudo-heatbath algorithm with over-relaxation. In a compound sweep, we perform one pseudo-heatbath sweep with three over-relaxation sweeps. For each  $\beta$ , over a thousand of gauge field configurations are generated, with each configuration separated by 3 compound sweeps mentioned above.

Using these gauge field configurations, Wilson loops are constructed and measured which yield static quark anti-quark potential. It is known that, Wilson loops, especially large loops are extremely noisy objects. We thus utilize the conventional smearing techniques for the spatial gauge links. In such a process, each spatial gauge link is replaced by its original value plus a linear combination of its nearest staples with a coefficient  $\lambda_s$ . Finally, each spatial gauge link is projected back into group  $SU(3)$ . Two different sets of smearing parameters are chosen for small spatial distance  $R$  and large  $R$ . Typically the smearing parameter in our simulations lies in the range:  $\lambda_s = 0.1 - 0.4$ . Smearing can be done iteratively. We usually perform 4 or 6 sweeps of smearing before our construction of the Wilson loops. Another useful technique is to use thermally averaged temporal links. This also greatly reduces the statistical errors.

The Wilson loops  $W(R, t)$  at a fixed spatial distance  $R$  and large temporal separation  $t$  is related to the static quark anti-quark potential  $V(R)$  by:

$$W(R, t) \simeq e^{-tV(R)} = e^{-\hat{t}\hat{V}(R)}, \quad t \rightarrow \infty. \quad (2)$$

Note that here we have used dimensionless temporal separation  $\hat{t} = t/a_t$  which assumes integral values. What is really measured is the dimensionless potential:  $\hat{V} = a_t V(R)$ . Within the range that we can reach in our simulation, we find that the potential can be well-represented by a linear term plus a Coulomb

term. Therefore, at various values of  $R$ , we fit the potential  $V(R)$  using the following form:

$$V(R) = V_0 + \frac{\alpha}{R} + \sigma R, \quad (3)$$

Or, in terms of the dimensionless potential:

$$\hat{V}(\hat{R}) = \hat{V}_0 + \frac{\hat{\alpha}}{\hat{R}} + \hat{\sigma}\hat{R}, \quad (4)$$

with  $\hat{V}_0 = a_t V_0$ ,  $\hat{\alpha} = \alpha a_t / a_s$ , and  $\hat{\sigma} = \sigma a_t a_s$ .

At this stage, we tried two ways of extracting the parameters  $\hat{\alpha}$  and  $\hat{\sigma}$ . In the first method, one first checks for plateau behaviors of ratios of Wilson loops between two neighboring  $\hat{t}$  in the large temporal region. According to Eq. (2), the height of these plateaus will give us the estimate for the dimensionless potential  $\hat{V}(\hat{R})$  for all values of  $\hat{R}$ . Then, in the second step, one fits the resulting  $\hat{V}(\hat{R})$  versus  $\hat{R}$  using Eq. (4). The result of this fit then gives the optimal values for  $\alpha$  and  $\sigma$ . In the second method, one directly performs a correlated fit for the on-axis Wilson loops using the form:

$$W(R, t) = Z(\hat{R}) \exp \left[ -\hat{t} \left( \hat{V}_0 + \frac{\hat{\alpha}}{\hat{R}} + \hat{\sigma}\hat{R} \right) \right], \quad (5)$$

Note that here all the  $Z(\hat{R})$  parameters plus the three parameters:  $\hat{V}_0$ ,  $\hat{\alpha}$  and  $\hat{\sigma}$  enters the fitting process.

In Fig. 1 and Fig. 2, we show the fit of the static potential for two different values of  $\beta$ . The dashed curves are the fits for the potential using the first method. For comparison purposes, potentials using the fitted parameters obtained with the second method are also plotted as the solid curves. The difference for the two methods is indistinguishable for large values of  $\beta$ . In any case, we find that the two methods always yield compatible results for the fitted parameters. We list in Table 1 the fitted parameters  $\hat{\alpha}$  and  $\hat{\sigma}$  for all  $\beta$  values together with the  $\chi^2$  per degree of freedom of the fit.

To set the scales of a lattice in physical unit, we use the so-called Sommer scale  $r_0$  defined as:

$$R^2 \left. \frac{dV(R)}{dR} \right|_{R=r_0} = 1.65. \quad (6)$$

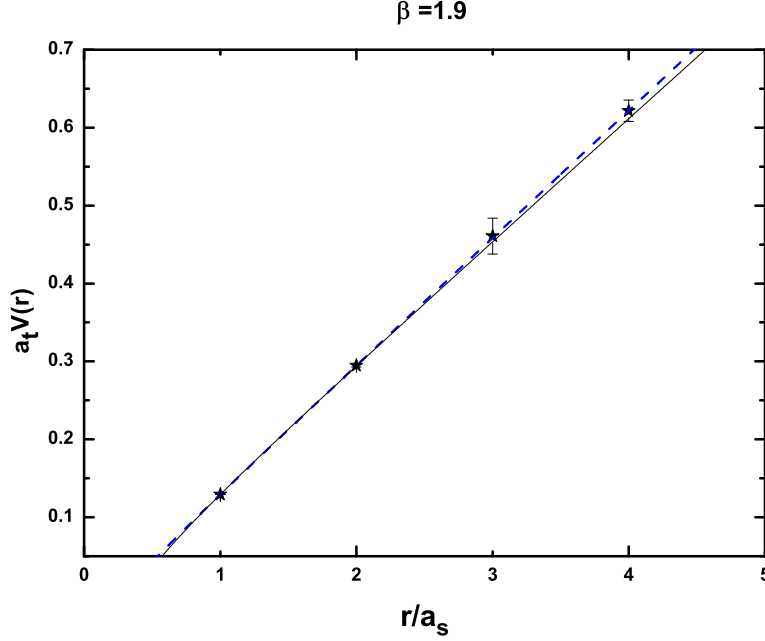


Fig. 1. The dimensionless potential  $\hat{V}(\hat{R})$  is fitted versus  $\hat{R}$  using Eq. (4) for  $\beta = 1.9$ . The dashed curve is the fit using the first method while the solid curve represents a direct fitting to the Wilson loops.

Table 1

Simulation parameters used in this work. All lattices are of size  $8^3 \times 40$  and  $\xi_0 = 5$ .

|                |            |            |            |            |            |
|----------------|------------|------------|------------|------------|------------|
| $\beta$        | 1.9        | 2.0        | 2.1        | 2.2        | 2.3        |
| $u_s^4$        | 0.328      | 0.345      | 0.361      | 0.377      | 0.394      |
| $\hat{\alpha}$ | -0.017(2)  | -0.021(2)  | -0.027(2)  | -0.030(1)  | 0.040(1)   |
| $\hat{\sigma}$ | 0.157(1)   | 0.1335(9)  | 0.1123(7)  | 0.0937(6)  | 0.0733(6)  |
| $\chi^2/d.o.f$ | 1.45       | 1.04       | 1.58       | 0.89       | 0.48       |
| $r_0/a_s$      | 1.415(12)  | 1.522(12)  | 1.644(16)  | 1.787(15)  | 1.991(18)  |
| $A$            | 14(2)      | 14(2)      | 14(2)      | 17(2)      | 20(2)      |
| $B$            | -44(7)     | -44(7)     | -44(7)     | -58(9)     | -71(11)    |
| $C$            | 39(8)      | 39(8)      | 39(8)      | 54(9)      | 69(12)     |
| $\beta$        | 2.4        | 2.5        | 2.6        | 2.7        | 2.8        |
| $u_s^4$        | 0.409      | 0.424      | 0.437      | 0.451      | 0.463      |
| $\hat{\alpha}$ | -0.0389(9) | -0.0407(6) | -0.0410(3) | -0.0599(5) | -0.0582(5) |
| $\hat{\sigma}$ | 0.0606(4)  | 0.0482(3)  | 0.0384(2)  | 0.0282(2)  | 0.0225(2)  |
| $\chi^2/d.o.f$ | 0.90       | 1.94       | 2.81       | 1.88       | 0.83       |
| $r_0/a_s$      | 2.191(17)  | 2.449(17)  | 2.743(11)  | 3.093(20)  | 3.476(23)  |
| $A$            | 23(2)      | 31(3)      | 34(3)      | 34(3)      | 34(3)      |
| $B$            | -88(11)    | -125(15)   | -142(16)   | -142(16)   | -142(16)   |
| $C$            | 88(13)     | 135(19)    | 155(20)    | 155(20)    | 155(20)    |

This implies that:

$$\frac{r_0}{a_s} = \sqrt{\frac{\alpha + 1.65}{\sigma a_s^2}} = \sqrt{\frac{\hat{\alpha} + 1.65/\xi}{\hat{\sigma}}}. \quad (7)$$

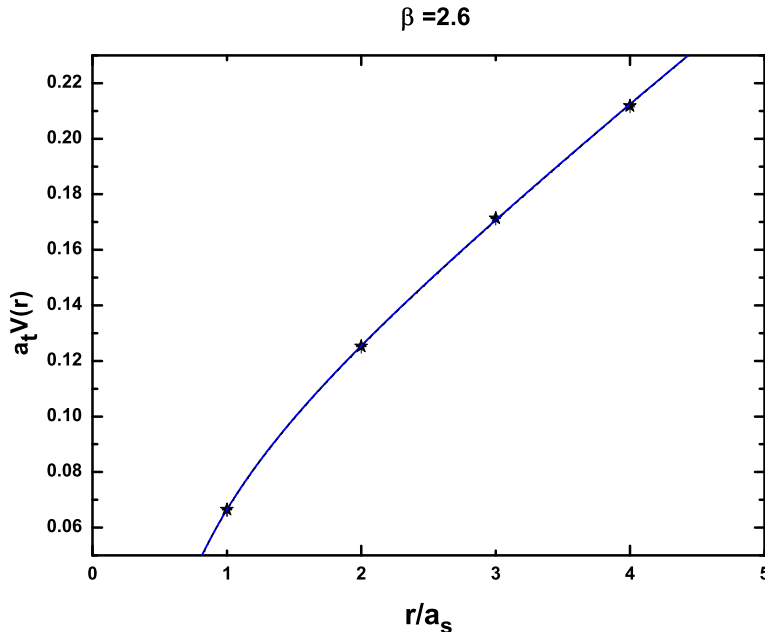


Fig. 2. Same as Fig. 1, but for  $\beta = 2.6$ .

where  $\xi = a_s/a_t$  is the (renormalized) anisotropy of the lattice. As we will verify, the renormalization effects for  $\xi_0$  are quite small, therefore we can replace  $\xi$  in the above expression by  $\xi_0$  in most cases. Also in Table 1, we list the values of  $(r_0/a_s)$  for various  $\beta$  values.

In order to obtain a one-to-one correspondence between  $\beta$  and  $r_0/a_s$  within the whole range we studied, we have also attempted to make interpolations within the whole range of  $\beta$  in our simulation. We use a five point quadratic fit in  $1/\beta$  around each point to interpolate points between the neighboring points of  $\beta$  that have been simulated:

$$\frac{r_0}{a_s} = A + \frac{B}{\beta} + \frac{C}{\beta^2}. \quad (8)$$

The situation is shown in Fig. 3. The data points are the resulting values of  $r_0/a_s$  obtained from the static quark potential at various values of  $\beta$ . The colored lines are the quadratic fitting curves around each simulated point. We see that these quadratic interpolations are smoothly connected with one another. Within each interval, different fitting curves agree within errors. For reference, we tabulated the fitted parameters  $A$ ,  $B$ ,  $C$  for each interpolation in Table 1. With these parameters, one can find the correspondence between  $\beta$  and the physical lattice spacing within the whole range of interest.

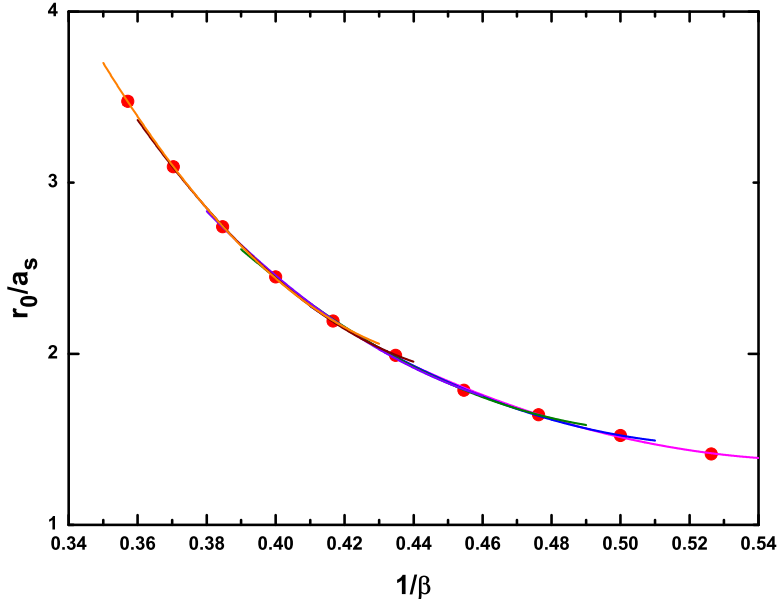


Fig. 3. Interpolations in the whole range of  $\beta$  that we simulated. Around each simulated point, we perform a five point quadratic interpolation around that point. These interpolations are shown as colored lines. It is seen that these lines interconnect each other well, showing that consistency of the interpolation.

### 3 Determination of renormalized anisotropy

We now move to the measurements of the anisotropy parameter  $\xi = a_s/a_t$ . This is a physical quantity which can be measured by various methods. In this work, we use the side-way potential method. The strategy for this method is briefly described below.

On anisotropic lattices, one can measure both the spatial-temporal Wilson loops and the spatial-spatial Wilson loops. Both of these objects contain information about the static quark anti-quark potential as a function of the quark distances. Since there is one unique physical potential, by comparing the results from these two measurements, one infers the information about physical anisotropy.

To be more precise, we assume that the spatial lattice axis are called  $x$ ,  $y$  and  $z$ , the temporal axis is called  $t$ . We can measure a spatial-temporal Wilson loop with the spatial separation  $\mathbf{R} = R\hat{z}$  lies in the  $z$  direction, with  $\hat{z}$  being a unit vector in the  $z$  direction. Since we are on a lattice, it is obvious that  $R = \hat{R}a_s$ , with  $\hat{R}$  being positive integers. If we measure the spatial-temporal Wilson loop  $W(\hat{R}a_s, \hat{t}a_t)$  and we investigate the large  $\hat{R}$  behavior of the loop,

we have:

$$W(Ra_s, ta_t) \propto e^{-\hat{R}a_s V_t(\hat{t}a_t)} , R \gg 1 . \quad (9)$$

Therefore, at large values of  $\hat{R}$ , we obtain the combination  $a_s V_t(\hat{t}a_t)$  for all values of  $\hat{t}$ . Here we use the notation  $V_t$  to indicate that it is a potential obtained from a spatial-temporal Wilson loop measurement.

On the other hand, we can also measure the spatial-spatial Wilson loop  $W(\hat{R}a_s, \hat{R}'a_s)$  with  $\hat{R}'a_s$  indicating the distance between the quark and anti-quark separation in the  $xy$  plane. We thus have:

$$W(\hat{R}a_s, \hat{R}'a_s) \propto e^{-\hat{R}a_s V_s(\hat{R}'a_s)} , R \gg 1 . \quad (10)$$

Again, for large enough  $\hat{R}$ , we obtain the potential  $a_s V_s(\hat{R}'a_s)$ . Here we use  $V_s$  to indicate that it is the potential from a spatial-spatial Wilson loop measurement. Note, however,  $V_t$  and  $V_s$  are in fact the same physical quantity. That is to say, if they evaluated at the same physical distance, they ought to be identical. Therefore, by measuring the spatial-spatial and spatial-temporal Wilson loops, we obtain two versions of the same potential. The renormalized anisotropy  $\xi$  has to be such that:

$$V(\hat{R}'a_s) = V\left(\frac{\hat{t}}{\xi}a_s\right) , \quad (11)$$

holds for all values of  $\hat{R}'$ .

To determine the anisotropy  $\xi$ , we plot  $a_s V(\frac{\hat{t}}{\xi}a_s)$  at all values of  $\hat{t}$  and interpolate in the whole range of  $\hat{t}$ . With this interpolation, a curve is obtained which gives the values of  $a_s V(\frac{\hat{t}}{\xi}a_s)$  versus  $\hat{t}$  continuously within the range. In the same plot, we draw horizontal lines with height of  $a_s V(\hat{R}'a_s)$  at various values of  $\hat{R}'$ . The crossing of these horizontal lines with the interpolation curve then offer the value of  $\hat{t}$  such that Eq. (11) is satisfied. This in turn gives an estimate for the value of  $\xi$ . This situation is demonstrated in Fig. 4. The data points are the results of  $a_s V(\frac{\hat{t}}{\xi}a_s)$  at different values of  $\hat{t}$ . The interpolation curve is also shown. Since our temporal lattice spacing is finer, usually linear interpolation is adequate. The horizontal dashed lines correspond to the values of  $a_s V(\hat{R}'a_s)$  at various values of  $\hat{R}'$ . The crossing points then finally give the results for the renormalized anisotropy.

The anisotropy obtained in this way depend weakly on the values of  $\hat{R}'$  chosen to make the connection. We choose to quote values of  $\xi$  obtained at  $\hat{R}' = 2$  as our final estimates since they are most stable and have less errors. Finally,



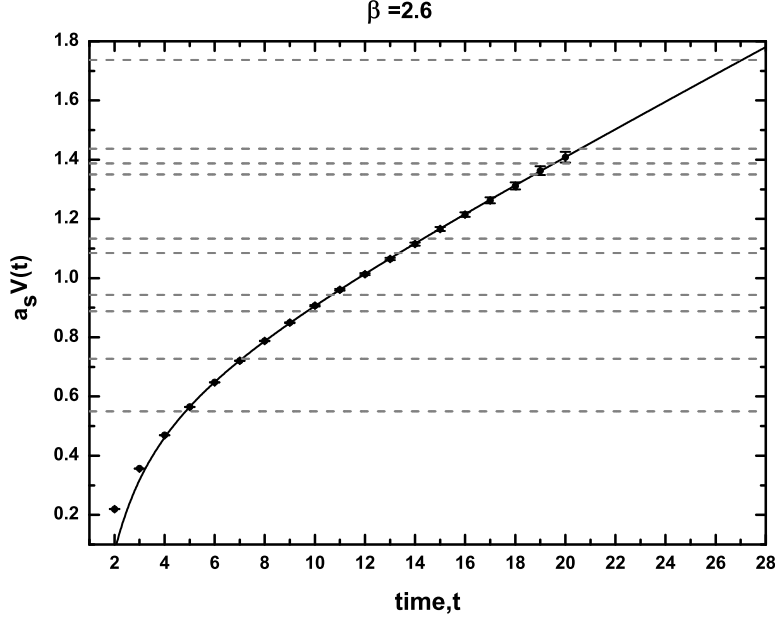


Fig. 4. Determination of physical anisotropy using the side-way potential method. This is the case for  $\beta = 2.6$ .

we can determine the physical anisotropy  $\xi$  for all values of  $\beta$  that have been simulated. In Fig. 5, we plot the ratio of the renormalized anisotropy to the bare anisotropy:  $\eta = \xi/\xi_0$  versus  $\beta$ . It is seen that the relative renormalization of the anisotropy parameter is very mild, less than a few percent, within the whole range of  $\beta$ . This is mainly due to tadpole improvement. It is known that at intermediate values of bare gauge coupling, the renormalization can be as large as 30% without tadpole improvement.

It is also interesting to compare our measured values with the result from perturbation theory. According to Ref. [11,12], the renormalized anisotropy can be well fitted with the formula:

$$\eta = \left( \frac{u_s}{u_t} \right) \left[ 1 + \left( 0.0955 - \frac{0.0702}{\chi_0} - \frac{0.0399}{\chi_0^2} \right) g_0^2 \right] , , \quad (12)$$

where the "boosted" bare coupling  $g_0^2$  and the boosted bare anisotropy  $\chi_0$  are given by:

$$\beta = \frac{6u_s^3 u_t}{g_0^2} , \quad \chi_0 = \xi_0 \frac{u_s}{u_t} . \quad (13)$$

In our simulation, we find  $u_t \simeq 1$  and when plugged into the above formulae, qualitative agreement between our measured values and the perturbative re-

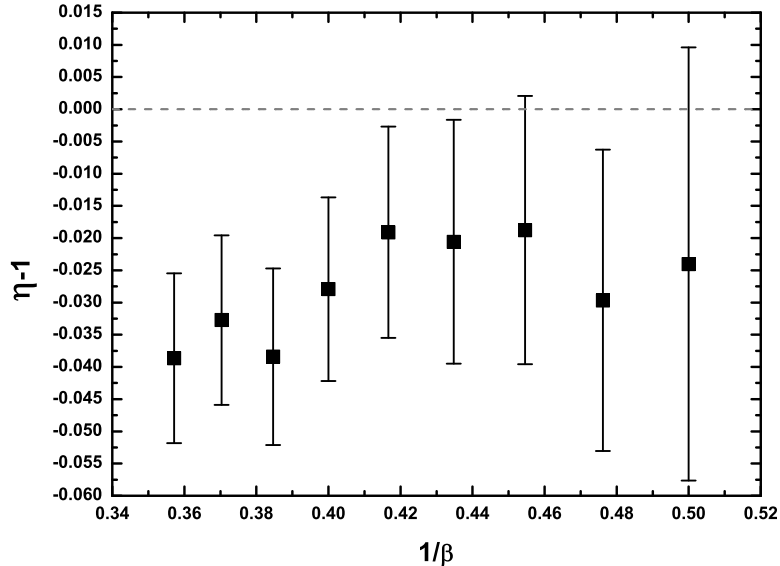


Fig. 5. The effects of renormalization for the anisotropy is shown. We plot  $\eta = \xi/\xi_0$  at various values of  $\beta$ , ranging between 1.9 and 2.8.

sults are found. However, our measured values of  $\eta$  are closer to unity than the predictions from perturbation theory.

## 4 Conclusions

In this paper, we present a numerical study of the static quark anti-quark potential using anisotropic lattice gauge action. Using the static quark potential obtained from Wilson loops, we determine the physical scale of the lattice spacing for a range of  $\beta$  values. This will set up a direct correspondence between the value of  $\beta$  and the physical lattice spacing. We also measure the renormalized anisotropy of the lattice using the side-way potential method. It is found that the renormalization effect for the anisotropy is small over the whole range of  $\beta$  that have been studied, typically below 5%. This is due to the use of tadpole improvement. The results obtained in this study will be useful for further applications of anisotropic lattices on other issues like the hadron-hadron scattering.

## Acknowledgments

We would like to thank Prof. H. Q. Zheng, Prof. S. L. Zhu and Prof. S.H. Zhu of Peking University for helpful discussions.

## References

- [1] G. P. Lepage and P. B. Mackenzie. *Phys. Rev. D*, 48:2250, 1993.
- [2] C. Morningstar and M. Peardon. *Phys. Rev. D*, 56:4043, 1997.
- [3] C. Morningstar and M. Peardon. *Phys. Rev. D*, 60:034509, 1999.
- [4] C. Liu. *Chinese Physics Letter*, 18:187, 2001.
- [5] C. Liu. *Communications in Theoretical Physics*, 35:288, 2001.
- [6] C. Liu. In *Proceedings of International Workshop on Nonperturbative Methods and Lattice QCD*, page 57. World Scientific, Singapore, 2001.
- [7] C. Liu and J. P. Ma. In *Proceedings of International Workshop on Nonperturbative Methods and Lattice QCD*, page 65. World Scientific, Singapore, 2001.
- [8] C. Liu. *Nucl. Phys. (Proc. Suppl.) B*, 94:255, 2001.
- [9] M. Alford, I.T. Drummond, R.R. Horgan, M. Peardon, and H. Shanahan. *Phys. Rev. D*, 63:074501, 2001.
- [10] S. Sakai and A. Nakamura. *Phys. Rev. D*, 69:114504, 2004.
- [11] I.T. Drummond, A. Hart, R.R. Horgan, and L.C. Storoni. *Phys. Rev. D*, 66:094509, 2002.
- [12] I.T. Drummond, A. Hart, R.R. Horgan, and L.C. Storoni. *Phys. Rev. D*, 68:057501, 2003.